JOURNAL OF COMPUTATIONAL PHYSICS 52, 524–544 (1983)

A Spectral Numerical Method for the Navier–Stokes Equations with Applications to Taylor–Couette Flow

R. D. MOSER

Department of Mechanical Engineering, Stanford University, Stanford, California 94305

AND

P. MOIN AND A. LEONARD

Ames Research Center, NASA, Moffett Field, California 94035

Received November 23, 1982

A new spectral method for solving the incompressible Navier–Stokes equations in a plane channel and between concentric cylinders is presented. The method uses spectral expansions which inherently satisfy the boundary conditions and the continuity equation and yield banded matrices which are efficiently solved at each time step. In addition, the number of dependent variables is reduced, resulting in a reduction in computer memory requirements. Several test problems have been computed for the channel flow and for flow between concentric cylinders, including Taylor–Couette flow with axisymmetric Taylor vortices and wavy vortices. In all cases, agreement with available experimental and theoretical results is very good.

1. INTRODUCTION

The purpose of this paper is to present a new spectral numerical method for simulating wall-bounded shear flows in Cartesian and cylindrical geometries. These flows have been under extensive theoretical and experimental investigation aimed at understanding the mechanics of transition and turbulence. Numerical simulations of these basic flows have become an important supplement to laboratory measurements. Among the problems that have been simulated are transition to turbulence in a channel [1, 2] and in pipes [3], the evolution of Taylor vortices in Taylor–Couette flow [4], and turbulent flow in a channel [5].

In these similations, spectral methods are often used to solve the incompressible Navier–Stokes equations

$$\frac{\partial \mathbf{u}}{\partial t} = -\nabla P - \frac{1}{\mathrm{Re}} \nabla \times \nabla \times \mathbf{u} + \mathbf{u} \times \boldsymbol{\omega}, \tag{1a}$$

$$\nabla \cdot \mathbf{u} = 0, \tag{1b}$$

0021-9991/83 $3.00

and

$$\mathbf{u} = 0 \qquad \text{at the walls,} \tag{1c}$$

where P is the dynamic pressure, Re is the Reynolds number, and $\boldsymbol{\omega}$ is the vorticity vector. Spectral methods are used because, for sufficiently smooth fields, they have a very high formal order of accuracy. This is particularly important in three-dimensional problems, in which the number of modes that can be used in each spatial direction is severely limited. However, spectral methods have proved difficult to apply to wall-bounded flows. The difficulty stems from the continuity equation (1b) and the no-slip boundary conditions (1c), which appear as constraints to the Navier–Stokes equations. When the dynamic equations (1a) are time-differenced, the continuity and boundary constraints must be imposed on the velocity field at each time-step. Moin and Kim [6] have shown that when spectral methods are used, the most common explicit time-differencing scheme leads to meaningless calculations, because the continuity and boundary conditions cannot be properly enforced. They suggest implicit time-differencing of the viscous and pressure terms to allow the imposition of the constraints.

Several schemes have been developed for the solution of Eqs. (1) using spectral methods. Most of these computations have used Fourier expansions in two space dimensions. In the method described by Moin and Kim [6], the velocity and pressure were expressed in terms of Chebychev polynomials (and Fourier functions). The momentum equations (1a) are time-differenced with viscous and pressure terms treated implicitly. The resulting equations are solved simultaneously with the continuity equation and the boundary condition equations for the Fourier–Chebychev coefficients. A nearly block-tridiagonal matrix results in the channel problem, in which Cartesian coordinates are used. It was found that in cylindrical coordinates a much more complicated matrix results, one that requires $750N$ operations to solve, where N is the number of radial modes.

In another aproach, Orszag and Kells [1] have used a fractional step scheme, using Chebychev polynomials, which seems to be quite efficient for the channel problem. Similar schemes have been used in cylindrical coordinates for flow in a pipe [3] and Taylor–Couette flow [4]; however, they result in matrices that are solved in $O(N^2)$ operations. In the fractional-step scheme used by these authors, each time-step is split into three independent "corrections." First, the nonlinear terms are explicitly time-advanced, yielding an intermediate field $\hat{\mathbf{v}}$. Then the pressure correction is applied, enforcing the continuity equation on the second intermediate field $\hat{\hat{\mathbf{v}}}$. Finally, the viscous correction is performed, allowing the imposition of the boundary conditions on the velocity field at the new time-step. Note that imposing the continuity constraint on the intermediate field $\hat{\mathbf{v}}$ leads to an error in the continuity equation of order $\Delta t/\mathrm{Re}$ for the final field. This appears to cause no serious problems in the channel calculations of Orszag and Kells; however, Marcus *et al.* [4] experienced some accuracy–stability problems related to the splitting when calculating Taylor–Couette flow.

A third method is given by Kleiser and Schumann [2], who have developed a

method for the channel problem using Chebychev polynomials. It requires the solution of three Helmholtz equations for the velocity components and a Poisson equation for the pressure. A procedure is used to determine the proper boundary conditions for the pressure to ensure satisfaction of the continuity equation. This method is quite efficient, though it has not yet been extended to non-Cartesian coordinates. Finally, Leonard [7] and Leonard and Wray [8] have recently developed a new method and applied it to flow in a pipe. A spectral representation based on Jacobi polynomials was used which inherently satisfies the continuity and boundary constraints.

In the method described in this paper, we follow Leonard [7] and represent the velocity field using vector functions which satisfy the continuity equation and boundary conditions. In this way, the constraints (1b) and (1c) are automatically satisfied. Satisfying the continuity equation also removes a degree of freedom, and since the pressure is eliminated from the equations only two dependent variables are left (in three-dimensional problems). Application of this method using Chebychev polynomials in Cartesian coordinates is described in Section 2. In Section 3 the method is developed for flow between concentric cylinders. In cylindrical coordinates, the resulting matrices are solved in $235N$ operations. Section 4 contains the results of some test problems used to verify the validity of the method.

2. Numerical Method in Cartesian Coordinates

In this section, a method for the numerical solution of the incompressible Navier–Stokes equations in a domain bounded by two parallel walls is presented. In the time advancement, the viscous term is treated implicitly, whereas an explicit scheme is used for the nonlinear (convective) terms. In this mixed explicit–implicit time-differencing, the explicitly treated terms act as a forcing term to the implicit part of the calculation. In essence, then, an implicit time-advancement procedure is needed for the forced Stokes equations (where the nonlinear term is replaced by a forcing term). It will be convenient in much of the discussion to follow to consider only the Stokes equations; however, the Navier–Stokes equations can be easily solved with any scheme for solving the Stokes equations, given a technique for computing $\mathbf{u} \times \boldsymbol{\omega}$.

Consider the forced Stokes equations,

$$\begin{aligned} &\frac{\partial \mathbf{v}}{\partial t} = -\nabla P - \frac{1}{\mathrm{Re}} \nabla \times \nabla \times \mathbf{v} + \mathbf{f}, \\ &\nabla \cdot \mathbf{v} = 0, \qquad \mathbf{v} = 0 \quad \text{at the walls,} \end{aligned} \tag{2}$$

where $\mathbf{v}$ is the velocity vector and $\mathbf{f}$ is some forcing function. It is assumed that the flow is periodic in the x and z directions and that the walls are located at $y = \pm 1$ (x, y, z are Cartesian coordinates; the cylindrical case will be discussed in Section 3).

2.1 *Velocity Representation*

A finite spatial representation of the velocity **v** is needed. Since **v** is constrained to satisfy the continuity equation and the boundary conditions, we choose a representation $\mathbf{v}_s$, which inherently satisfies these constraints.

$$\begin{aligned} \mathbf{v}_s(x, y, z, t) &= \sum_{k_x} \sum_{k_z} \sum_{l=0}^{L} \alpha_{jml}(t)\, \mathbf{w}_{jml}(x, y, z), \\ \mathbf{w}_{jml}(x, y, z) &= \mathbf{u}_l(y; k_x, k_z)\, e^{ik_x x} e^{ik_z z}, \end{aligned} \tag{3}$$

where

$$k_x = \frac{j2\pi}{L_x}, \quad -J \leqslant j \leqslant J, \qquad k_z = \frac{m2\pi}{L_z}, \quad -M \leqslant m \leqslant M \tag{4}$$

are the wave numbers, L_x, L_z are the periods in x and z, respectively, $\alpha_{jml}(t)$ are the coefficients of the expansion, and $\mathbf{u}_l(y)$ are a set of vector functions chosen to satisfy

$$\nabla \cdot \mathbf{w}_{jml} = 0, \qquad \mathbf{u}_l(y = \pm 1) = 0. \tag{5}$$

The representation must also be complete so that for sufficiently large J, M, and L, all vector fields of interest can be represented by (3).

Substituting the representation (3) into the Stokes equations (2), one obtains ordinary differential equations for the coefficients $\alpha_{jml}(t)$. This is accomplished by using a weighted residual method which involves dot multiplying the equations by a set of weight vectors and integrating over the computational domain. Vector weight functions $\boldsymbol{\phi}_{j',m',l'}$ are chosen as follows:

$$\boldsymbol{\phi}_{j',m',l'} = \boldsymbol{\xi}_{l'}(y; k_x, k_z)\, e^{-ik_x x} e^{-ik_z z}, \tag{6}$$

with

$$\nabla \cdot \boldsymbol{\phi}_{j',m',l'} = 0, \qquad \boldsymbol{\xi}_{l'}(y = \pm 1) \cdot \mathbf{n} = 0, \tag{7}$$

where **n** is a unit vector normal to the walls. When the weight vectors are formed in this way, it can be shown, using integration by parts, that the pressure term is eliminated from the resulting equations.

After using the orthogonality property of the complex exponential to evaluate the x and z portion of the integrals, the weighted residual method yields the following set of equations for each wave-number set k_x, k_z:

$$\sum_{l=0}^{L} \frac{d\alpha_l}{dt} \int_{-1}^{1} \boldsymbol{\xi}_{l'} \cdot \mathbf{u}_l \, dy = -\frac{1}{\mathrm{Re}} \sum_{l=0}^{L} \alpha_l \int_{-1}^{1} \boldsymbol{\xi}_{l'} \cdot \widehat{\nabla \times \nabla \times \mathbf{u}_l} \, dy + \int_{-1}^{1} \boldsymbol{\xi}_{l'} \cdot \hat{\mathbf{f}} \, dy, \tag{8}$$

where $\boldsymbol{\xi}_{l'}$ and $\mathbf{u}_l$ depend parametrically on k_x and k_z, $\hat{\mathbf{f}}$ is the Fourier transform of **f**,

and $\widehat{\nabla\times}$ is the Fourier transformed curl operator. Note that the subscripts j and m have been dropped for brevity. These equations can be written in the compact form

$$A\frac{d\boldsymbol{\alpha}}{dt}=\frac{1}{\mathrm{Re}}B\boldsymbol{\alpha}+\mathbf{F}, \tag{9}$$

where A and B are $(L+1)\times(L+1)$ matrices with elements

$$\begin{aligned} A_{l',l}&=\int_{-1}^{1}\boldsymbol{\xi}_{l'}\cdot\mathbf{u}_l\,dy,\\ B_{l',l}&=-\int_{-1}^{1}\boldsymbol{\xi}_{l'}\cdot\widehat{\nabla\times\nabla\times}\,\mathbf{u}_l\,dy, \end{aligned} \tag{10}$$

$\boldsymbol{\alpha}$ is the vector with elements α_l, and $\mathbf{F}$ is the vector with elements

$$F_{l'}=\int_{-1}^{1}\boldsymbol{\xi}_{l'}\cdot\hat{\mathbf{f}}\,dy. \tag{11}$$

Equation (9) is a system of linear ordinary differential equations which can be solved numerically using any standard time-discretization scheme. However, it should be noted that even an explicit scheme will require the "inversion" of the matrix A; therefore, unless A is much more sparse than B, there is no computational advantage in using an explicit scheme.

The method described above can also be derived from the variational formulation of the Stokes equations (see [9]). Consideration of the variational form leads to the conclusion that the weight functions $\boldsymbol{\phi}$, as well as the velocity representation functions $\mathbf{w}$, must satisfy a completeness condition. It can also be shown using projection arguments that a special case of the method presented here (where the vectors $\boldsymbol{\phi}$ and $\mathbf{w}$ are the same) yields a solution to the Stokes equation which has minimum square error in the vorticity.

2.2 *Choosing Vector Functions*

We now turn to the problem of choosing the vectors $\boldsymbol{\xi}_{l'}$ and $\mathbf{u}_l$. There is considerable freedom in this choice. The vectors presented here were constructed to yield matrices A and B in Eq. (9) which are banded with small bandwidths. This is easily accomplished when one of the wave numbers (say k_z) is zero. First, vectors will be constructed for this special case; later the results will be extended to the general case.

It becomes necessary to split the sets of vectors $\boldsymbol{\xi}$ and $\mathbf{u}$ into two classes $(\boldsymbol{\xi}^+,\boldsymbol{\xi}^-)$ and $(\mathbf{u}^+,\mathbf{u}^-)$, respectively, each class having a different functional form. This is equivalent to independently representing two components of the velocity vector, with the third determined by the continuity equation. To obtain tightly banded matrices,

we desire that the equations for $\mathbf{u}^+$ be decoupled from the equations for $\mathbf{u}^-$, that is,

$$\begin{aligned} &\int_{-1}^{1} \boldsymbol{\xi}_{l'}^{+} \cdot \mathbf{u}_l^{-}\, dy = 0, \qquad \int_{-1}^{1} \boldsymbol{\xi}_{l'}^{+} \cdot \widehat{\nabla \times \nabla \times \mathbf{u}_l^{-}}\, dy = 0, \\ &\int_{-1}^{1} \boldsymbol{\xi}_{l'}^{-} \cdot \mathbf{u}_l^{+}\, dy = 0, \qquad \int_{-1}^{1} \boldsymbol{\xi}_{l'}^{-} \cdot \widehat{\nabla \times \nabla \times \mathbf{u}_l^{+}}\, dy = 0. \end{aligned} \tag{12}$$

A convenient choice which satisfies this requirement (for $k_z = 0$) is

$$\begin{aligned} \mathbf{u}_l^{+} &= \begin{pmatrix} u_x \\ u_y \\ u_z \end{pmatrix} = \begin{pmatrix} ig_l' \\ k_x g_l \\ 0 \end{pmatrix}, \qquad \mathbf{u}_l^{-} = \begin{pmatrix} 0 \\ 0 \\ h_l \end{pmatrix}, \\ \boldsymbol{\xi}_{l'}^{+} &= \begin{pmatrix} \xi_x \\ \xi_y \\ \xi_z \end{pmatrix} = \begin{pmatrix} -iQ_{l'}' \\ k_x Q_{l'} \\ 0 \end{pmatrix}, \qquad \boldsymbol{\xi}_{l'}^{-} = \begin{pmatrix} 0 \\ 0 \\ P_{l'} \end{pmatrix}, \end{aligned} \tag{13}$$

where g, Q, h, and P are indexed functions of y to be chosen later, and the superscript primes indicate differentiation with respect to y. It can be easily verified that these vectors satisfy the continuity conditions (5) and (7); the boundary conditions will be satisfied if

$$\begin{aligned} &g_l(y = \pm 1) = 0, \qquad h_l(y = \pm 1) = 0, \\ &g_l'(y = \pm 1) = 0, \qquad Q_{l'}(y = \pm 1) = 0. \end{aligned} \tag{14}$$

The integrals in Eqs. (10) can be evaluated by using the identity in Cartesian coordinates (for $\nabla \cdot \mathbf{u} = 0$),

$$\nabla \times \nabla \times \mathbf{u} = -\nabla^2 \mathbf{u}, \tag{15}$$

and integrating by parts, with the results

$$\begin{aligned} A_{l',l}^{+} &= \int_{-1}^{1} \boldsymbol{\xi}_{l'}^{+} \cdot \mathbf{u}_l^{+}\, dy = -\int_{-1}^{1} Q_{l'}(\mathscr{L} g_l)\, dy, \\ B_{l',l}^{+} &= -\int_{-1}^{1} \boldsymbol{\xi}_{l'}^{+} \cdot (\widehat{\nabla \times \nabla \times \mathbf{u}_l^{+}})\, dy = -\int_{-1}^{1} (\mathscr{L} Q_{l'})(\mathscr{L} g_l)\, dy, \\ A_{l',l}^{-} &= \int_{-1}^{1} \boldsymbol{\xi}_{l}^{-} \cdot \mathbf{u}_l^{-}\, dy = \int_{-1}^{1} P_{l'} h_l\, dy, \end{aligned} \tag{16}$$

and

$$B^-_{l',l} = -\int_{-1}^{1} \xi^-_{l'} \cdot (\widehat{\nabla \times \nabla \times \mathbf{u}^-_l})\, dy = \int_{-1}^{1} P_{l'}(\mathscr{L} h_l)\, dy,$$

where $\mathscr{L}$ is the Fourier-transformed Laplacian operator.

$$\mathscr{L} = \frac{d^2}{dy^2} - k_x^2. \tag{17}$$

Therefore, when the vectors (13) are used, Eq. (9) is decomposed into two independent equations for the $\mathbf{u}^+$ and $\mathbf{u}^-$ coefficients,

$$A^+ \frac{d\boldsymbol{\alpha}^+}{dt} = \frac{1}{\mathrm{Re}} B^+ \boldsymbol{\alpha}^+ + \mathbf{F}^+, \tag{18a}$$

$$A^- \frac{d\boldsymbol{\alpha}^-}{dt} = \frac{1}{\mathrm{Re}} B^- \boldsymbol{\alpha}^- + \mathbf{F}^-, \tag{18b}$$

with matrices as defined in (16) and $\mathbf{F}^+$ and $\mathbf{F}^-$ defined as follows:

$$\begin{aligned} F^+_{l'} &= \int_{-1}^{1} (k_x Q_{l'} \hat{f}_y - i Q'_{l'} \hat{f}_x)\, dy, \\ F^-_{l'} &= \int_{-1}^{1} P_{l'} \hat{f}_z\, dy. \end{aligned} \tag{19}$$

It should be mentioned that in Cartesian coordinates Eqs. (18) can be derived in a more straightforward way (this will not be the case in cylindrical coordinates; see Section 3). Equation (18b) is readily obtained from the z equation of (2), after Fourier transforming (again $k_z = 0$),

$$\frac{\partial \hat{v}_z}{\partial t} = \frac{1}{\mathrm{Re}} \mathscr{L} \hat{v}_z + \hat{f}_z. \tag{20}$$

If the representation

$$\hat{v}_z = \sum_{l=0}^{L/2} \alpha^-_l h_l \tag{21}$$

is used in a weighted residual method with weights $P_{l'}$, Eq. (18b) is obtained. For Eq. (18a), the curl operator is used twice on (2), which yields

$$\frac{\partial}{\partial t} (\nabla \times \nabla \times \mathbf{v}) = -\frac{1}{\mathrm{Re}} (\nabla \times)^4 \mathbf{v} + \nabla \times \nabla \times \mathbf{f}. \tag{22}$$

After Fourier transforming and using (15), the y equation of (22) is the fourth-order equation

$$-\frac{\partial}{\partial t}(\mathscr{L}\hat{v}_y) = -\frac{1}{\mathrm{Re}}(\mathscr{L}^2\hat{v}_y) + (\widehat{\nabla \times \nabla \times \mathbf{f}})_y. \tag{23}$$

The representation

$$\hat{v}_y = \sum_{l=0}^{L/2} a_l^+ g_l \tag{24}$$

and the weight functions $Q_{l'}$ yield Eq. (18a). The continuity equation evaluated at the walls requires

$$\frac{\partial v_y}{\partial y}(y = \pm 1) = 0, \tag{25}$$

which provides the additional boundary conditions on v_y to make Eq. (23) well posed. The x velocity is determined from the continuity equation. Thus, for this case, solution of (2) after Fourier transforming is equivalent to the solution of (20) and (23). Equations (20) and (23) were solved in a method used by Patera and Orszag [10].

Extension of the vectors used above to the general case when $k_x \neq 0$ and $k_z \neq 0$ is straigthforward. By rotating the coordinate system about the y axis, the general problem can be reduced to the $k_z = 0$ case already discussed. The new axes (x' and z') are rotated such that the x' axis is aligned with the vector

$$k_x \mathbf{e}_x + k_z \mathbf{e}_z,$$

where $\mathbf{e}_x$ and $\mathbf{e}_z$ are unit vectors in the x and z directions. Then

$$k_{x'} = (k_x^2 + k_z^2)^{1/2}, \qquad k_{z'} = 0, \tag{26}$$

and the vectors (13) can be used. This is the coordinate transformation at the heart of Squire's theorem in the hydrodynamic stability of plane parallel shear flows [11].

Finally, the vectors defined in (13) are incomplete when both k_x and k_z are zero. For this case, the following set of vectors is used:

$$\mathbf{u}_l^+ = \begin{pmatrix} h_l \\ 0 \\ 0 \end{pmatrix}, \qquad \mathbf{u}_l^- = \begin{pmatrix} 0 \\ 0 \\ h_l \end{pmatrix},$$
$$\boldsymbol{\xi}_{l'}^+ = \begin{pmatrix} P_{l'} \\ 0 \\ 0 \end{pmatrix}, \qquad \boldsymbol{\xi}_{l'}^- = \begin{pmatrix} 0 \\ 0 \\ P_{l'} \end{pmatrix}. \tag{27}$$

This leads to identical matrices for the plus and minus equations; the derivation follows that for Eq. (18b).

2.3 *Quasi-orthogonal Functions*

The expansion functions Q, g, h, and P must now be chosen. Strictly orthogonal functions [which would lead to diagonal matrices A and B in (18)] should not be used, because requiring orthogonal functions to satisfy boundary conditions (14) imposes extraneous conditions on higher derivatives of the functions, which degrades the rapid convergence of the method [12]. Instead, we use quasi-orthogonal functions, which lead to banded matrices A and B, and do not suffer from this convergence problem. Quasi-orthogonal functions are constructed from a set of orthogonal functions which admit general boundary conditions (see [12] for a discussion of this class of functions). Since these functions do not inherently satisfy any boundary conditions, boundary conditions are imposed by forming linear combinations of them to make the quasi-orthogonal function. This construction must be done in such a way as to make the matrices A and B, which involve integrals of the functions and their derivatives, banded. Orthogonal polynomials are suitable for this purpose, because they satisfy recursion relations which make this construction easier.

The Chebychev polynomials have been chosen for this application because they have two properties that are particularly useful.

(1) They are related to the cosine function through a coordinate transformation [13]; this allows the use of the fast Fourier transform in evaluating **F**.

(2) They are particularly efficient for resolving boundary layers near the walls ($y = \pm 1$) [12].

The quasi-orthogonal functions g, Q, P, h are constructed as follows:

$$
\begin{aligned}
&g_l = (1-y^2)^2\, T_l(y), \qquad h_l = (1-y^2)\, T_l(y),\\
&Q_l = \left(\frac{T_{l+2}}{l(l+1)} - \frac{2T_l}{(l+1)(l-1)} + \frac{T_{l-2}}{l(l-1)}\right) \Big/ 4(1-y^2)^{1/2},\\
&P_l = (T_{l-1} - T_{l+1})/2l(1-y^2)^{1/2},
\end{aligned}
\tag{28}
$$

where T_l is the Chebychev polynomial of order l and the factor $1/(1-y^2)^{1/2}$ appearing in Q and P is the weight function for the Chebychev orthogonality relation. These functions have been constructed so that they and their derivatives have simple forms when expressed as linear combinations of Chebychev polynomials, which guarantees that the matrices A and B are banded.

Other orthogonal polynomials can be used to construct quasi-orthogonal functions. This is a consequence of the recursion and differential relationships that orthogonal polynomials satisfy (the Chebychev relationships are particularly simple). Thus there are many possible sets of quasi-orthogonal functions that can be used to meet requirements that might be imposed in a given problem. For example, Leonard and

Wray [8] have used functions based on shifted Jacobi polynomials to satisfy certain constraints in the calculation of flow in a pipe.

With the choices of the functions Q, g, P, h, the method is completely defined. Of great interest is the amount of computation required to implement this method. After taking advantage of the decoupling of even and odd functions, both matrices A^+ and B^+ have seven nonzero diagonals of which two are subdiagonals and four are superdiagonals, A^- and B^- have four nonzero diagonals, one being a subdiagonal and two being superdiagonals. Also, the elements in the matrices depend only on the square of the wave numbers k_x and k_z so that at least two wave-number sets can be solved simultaneously. The result is that for each wave-number set k_x, k_z, the matrices arising from an implicit time-differencing of Eqs. (18) can be solved in $30N$ real additions and multiplications, where N is the number of $\mathbf{u}^+$ vectors used (three less than the highest-order Chebychev polynomial used). There is some additional computation required to calculate the forcing vector $\mathbf{F}$ and to perform the coordinate rotations discussed earlier. The total cost is then $50N$ operations. Thus the method is operationally efficient, in addition to offering savings in computer storage by reducing the number of independent variables.

3. Application to Cylindrical Coordinates

The concepts presented in Section 2 will now be applied in cylindrical coordinates to the solution of Eq. (2). We shall consider the flow in an annulus. In this case the flow is periodic in the axial (z) direction and the azimuthal (θ) direction. The inner and outer walls are located at $r = r_i$ and $r = r_o$, respectively. Using representations and weight vectors as in (3) and (6), a result (for cylindrical coordinates) similar to (8) is obtained:

$$\sum_{l=0}^{L} \frac{d\alpha_l}{dt} \int_{r_i}^{r_o} \boldsymbol{\xi}_{l'} \cdot \mathbf{u}_l r\, dr = -\frac{1}{\mathrm{Re}} \sum_{l=0}^{L} \alpha_l \int_{r_i}^{r_o} \boldsymbol{\xi}_{l'} \cdot \widehat{\nabla \times \nabla \times \mathbf{u}_l} r\, dr + \int_{r_i}^{r_o} \boldsymbol{\xi}_{l'} \cdot \hat{\mathbf{f}} r\, dr, \tag{29}$$

where $\boldsymbol{\xi}_l(r)$ and $\mathbf{u}_l(r)$ depend parametrically on k_θ and k_z, the θ and z wave numbers. The equations can be written as

$$A \frac{d\boldsymbol{\alpha}}{dt} = \frac{1}{\mathrm{Re}} B\boldsymbol{\alpha} + \mathbf{F}, \tag{30}$$

where A and B are matrices with elements.

$$\begin{aligned} A_{l',l} &= \int_{r_i}^{r_o} \boldsymbol{\xi}_{l'} \cdot \mathbf{u}_l r\, dr, \\ B_{l',l} &= -\int_{r_i}^{r_o} \boldsymbol{\xi}_{l'} \cdot \widehat{\nabla \times \nabla \times \mathbf{u}_l} r\, dr, \end{aligned} \tag{31}$$

and **F** is the forcing vector,

$$F_{l'} = \int_{r_i}^{r_0} \xi_{l'} \cdot \hat{\mathbf{f}} r \, dr. \tag{32}$$

Again, it is desirable to choose ξ and $\mathbf{u}$ to make the matrices A and B tightly banded. The first step is to attempt to uncouple the equations for the two sets of vectors ξ^+, $\mathbf{u}^+$, and ξ^-, $\mathbf{u}^-$. In cylindrical coordinates, however, the appearance of u_θ in the r-component of $\nabla \times \nabla \times \mathbf{u}$ (for $\nabla \cdot \mathbf{u} = 0$) and u_r in the θ component makes the decoupling more difficult than in the Cartesian case.

The following vectors satisfy the decoupling requirement, though they have an important defect to be discussed later.

$$\mathbf{u}_l^+ = \begin{pmatrix} u_r^+ \\ u_\theta^+ \\ u_z^+ \end{pmatrix}_l = \widehat{\nabla\times} \begin{pmatrix} ig_l \\ g_l \\ 0 \end{pmatrix} = \begin{pmatrix} -ik_z g_l \\ -k_z g_l \\ g_l' + \dfrac{k_\theta + 1}{r} g_l \end{pmatrix}, \qquad \xi_{l'}^+ = \widehat{\nabla \times \nabla\times}^* \begin{pmatrix} -iQ_{l'} \\ Q_{l'} \\ 0 \end{pmatrix}, \tag{33}$$

$$\mathbf{u}_l^- = \widehat{\nabla\times} \begin{pmatrix} -ig_l \\ g_l \\ 0 \end{pmatrix} = \begin{pmatrix} -ik_z g_l \\ k_z g_l \\ g_l' + \dfrac{1 - k_\theta}{r} g_l \end{pmatrix}, \qquad \xi_{l'}^- = \widehat{\nabla \times \nabla\times}^* \begin{pmatrix} iQ_{l'} \\ Q_{l'} \\ 0 \end{pmatrix},$$

where $Q_{l'}$ and g_l are indexed functions of r [not the same as in (28)], and $\widehat{\nabla\times}^*$ is the complex conjugate Fourier transformed curl operator. Satisfaction of the continuity equation is guaranteed by the identity $\nabla \cdot (\nabla \times \mathbf{u}) = 0$. In order to enforce the

[redacted]

$$g_l'(r = r_i, r_0) = 0, \qquad Q_l'(r = r_i, r_0) = 0. \tag{34}$$

Equation (30) now decomposes into two equations, as in (18). However, the vector functions defined in (33) are an incomplete set, because the imposition of boundary conditions in (34) forces the θ-velocity to satisfy the condition

$$\frac{\partial u_\theta}{\partial r} = 0, \qquad \text{at} \qquad r = r_i, r_0 \tag{35}$$

which is too restrictive. To alleviate this problem, the vectors in (33) are augmented with two extra vectors,

$$\mathbf{u}_l^0 = \begin{pmatrix} 0 \\ -2k_z h_l \\ (2k_\theta / r) h_l \end{pmatrix}, \qquad \xi_{l'}^0 = \begin{pmatrix} ik_\theta P_{l'} \\ rP_l' + P_{l'} \\ 0 \end{pmatrix}, \tag{36}$$

where l and l' can be 0 or 1. With this addition, $\partial u_\theta/\partial r$ can have arbitrary values at the walls. When the extra vectors are included, Eqs. (18a) and (18b) become

$$A_+^+ \frac{d\boldsymbol{\alpha}^+}{dt} + A_0^+ \frac{d\boldsymbol{\alpha}^0}{dt} = \frac{1}{\mathrm{Re}} (B_+^+ \boldsymbol{\alpha}^+ + B_0^+ \boldsymbol{\alpha}^0) + \mathbf{F}^+, \tag{37a}$$

$$A_-^- \frac{d\boldsymbol{\alpha}^-}{dt} + A_0^- \frac{d\boldsymbol{\alpha}^0}{dt} = \frac{1}{\mathrm{Re}} (B_-^- \boldsymbol{\alpha}^- + B_0^- \boldsymbol{\alpha}^0) + \mathbf{F}^-, \tag{37b}$$

$$A_+^0 \frac{d\boldsymbol{\alpha}^+}{dt} + A_-^0 \frac{d\boldsymbol{\alpha}^-}{dt} + A_0^0 \frac{d\boldsymbol{\alpha}^0}{dt} = \frac{1}{\mathrm{Re}} (B_+^0 \boldsymbol{\alpha}^+ + B_-^0 \boldsymbol{\alpha}^- + B_0^0 \boldsymbol{\alpha}^0) + \mathbf{F}^0, \tag{37c}$$

where the matrices are defined as

$$\begin{aligned} (A_\beta^\gamma)_{l',l} &= \int_{r_i}^{r_o} \boldsymbol{\xi}_{l'}^\gamma \cdot \mathbf{u}_l^\beta r \, dr, \\ (B_\beta^\gamma)_{l',l} &= -\int_{r_i}^{r_o} \boldsymbol{\xi}_{l'}^\gamma \cdot \widehat{\nabla \times \nabla \times} \, \mathbf{u}_l^\beta r \, dr. \end{aligned} \tag{38}$$

The subscripts–superscripts γ and β can be $+$, $-$, or 0. The equations in (37) are coupled, but in a weak way that will not appreciably affect the computational efficiency of the method (see below).

The functions Q, g, P, and h are again constructed with Chebychev polynomials,

$$\begin{aligned} g_l &= r(1-y^2)^2 \, T_l(y), \qquad h_l = r(1-y^2) \, T_l(y), \\ Q_l &= \frac{r^2}{(1-y^2)^{1/2}} \left(\frac{T_{l-2}}{4(l-1)\,l} - \frac{T_l}{2(l-1)(l+1)} + \frac{T_{l+2}}{4(l+1)\,l} \right), \\ P_l &= (T_{l-1} - T_{l+1})/2l(1-y^2)^{1/2}, \end{aligned} \tag{39}$$

where

$$y = \frac{2r - r_o - r_i}{r_o - r_i},$$

so that y is -1 where $r = r_i$ and $+1$ where $r = r_o$. These are the same functions used in the Cartesian problem, except for the factors of r and r^2. These factors are included to cancel the various $1/r$'s appearing in the $\mathscr{L}$ operators, which is necessary if the Chebychev orthogonality relations are to be used to evaluate the integrals in Eqs. (38).

The coupled equations (37a)–(37c) can be written as a single equation, as in (30) ($\boldsymbol{\alpha}$ is composed of the vectors $\boldsymbol{\alpha}^+$, $\boldsymbol{\alpha}^-$, $\boldsymbol{\alpha}^0$). The resulting matrices A and B have the special form shown in Fig. 1. Also shown are the bandwidths for the various nonzero bands in the submatrices. Though this matrix is not strictly banded, it can be solved with no difficulty. As in the Cartesian case, there are wave-number symmetries which

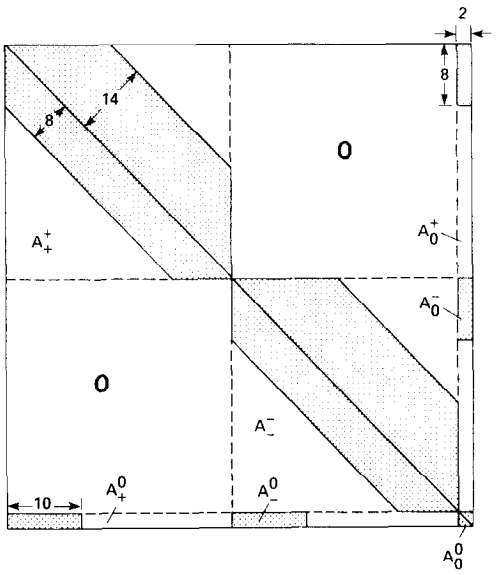

FIG. 1. Structure of matrix A (B is identical). Submatrices shown are as defined in (38). Shaded areas indicate nonzero elements, and dimensions refer to numbers of rows, columns, or diagonals.

allow the solution of more than one wave-number set at a time. Including these symmetries, the operation count for the matrix solution for each wave-number set k_θ, k_z is $235N$ additions and multiplications, where N is the number of $\mathbf{u}^+$ vectors (four fewer than the highest order Chebychev polynomials used).

The representation presented above is incomplete when $k_z = 0$. The following vectors are used for the special case $k_z = 0$, $k_\theta \neq 0$.

$$\mathbf{u}_l^+ = \begin{pmatrix} -\dfrac{ik_\theta g_l}{r} \\ g_l' \\ 0 \end{pmatrix}, \qquad \boldsymbol{\xi}_l^+ = \begin{pmatrix} \dfrac{ik_\theta}{r} Q_l \\ Q' \\ 0 \end{pmatrix},$$
$$\mathbf{u}_l^- = \begin{pmatrix} 0 \\ 0 \\ h_l \end{pmatrix}, \qquad \boldsymbol{\xi}_l^- = \begin{pmatrix} 0 \\ 0 \\ P_l \end{pmatrix}, \tag{40}$$

where Q, g, P, and h are as defined in (43). When $k_z = 0$ and $k_\theta = 0$, the vectors in (40) are incomplete. In this case the following vectors are used:

$$\mathbf{u}_l^+ = \begin{pmatrix} 0 \\ h_l \\ 0 \end{pmatrix}, \qquad \boldsymbol{\xi}_l^+ = \begin{pmatrix} 0 \\ P_l \\ 0 \end{pmatrix},$$
$$\mathbf{u}_l^- = \begin{pmatrix} 0 \\ 0 \\ h_l \end{pmatrix}, \qquad \boldsymbol{\xi}_l^- = \begin{pmatrix} 0 \\ 0 \\ P_l \end{pmatrix}, \tag{41}$$

The vectors in (40) and (41) are very similar to the ones used in the Cartesian case and lead to uncoupled sets of equations. Solution for these cases requires less computation than the general case considered above.

4. Numerical Results

The numerical methods described in Sections 2 and 3 have been applied to several problems. In all cases, the Navier–Stokes equations were solved by replacing the forcing function in Eq. (2) with the nonlinear terms evaluated using the pseudospectral technique (collocation). Crank–Nicholson time-differencing was used for the viscous terms, and Adams–Bashforth was used for the nonlinear terms. For the problems in Subsection 4.2, the nonlinear terms were computed by collocation on a grid large enough to eliminate aliasing.

4.1 *Cartesian Test Cases*

To test the Cartesian version of the method (Section 2), the evolution of an oblique decaying Tollmien–Schlichting wave in a channel was computed. The computation was done for $\mathrm{Re} = 1500$, $k_x = 1$, and $k_z = 1$, where Reynolds number is based on centerline velocity and channel half-width. Chebychev polynomials through order 32 were used. Initial conditions for the computation were obtained from an Orr–Sommerfield eigenfunction program [14]. The amplitude of the disturbance was initially set to 10^{-5} so linear disturbance theory was applicable. The wave was allowed to evolve for 3.9 nondimensional time units (40 time-steps), at which time the decay rate was within 0.2% of that obtained from linear theory, and the propagation velocity was within 0.05%.

4.2 *Cylindrical Test Cases*

The cylindrical version of the method (Section 3) was used to compute the flow between concentric cylinders with the inner cylinder rotating (Taylor–Couette flow). For sufficiently high Reynolds numbers, Taylor–Couette flow consists of counter-rotating, axisymmetric, toroidal vortices with a range of possible wavelengths. At still higher Reynolds numbers, these vortices become nonaxisymmetric (wavy) with several possible azimuthal wavelengths (see [15, 16]). Five axisymmetric problems and three nonaxisymmetric problems have been computed. The results for the

axisymmetric cases are compared to the finite-difference calculations of Meyer [17], the experiments of Donnelly and Simon [18], and the stability analysis of DiPrima and Eagles [19]. The three-dimensional cases are compared to the experiments of Coles [15] and the stability analysis of Jones [20].

The first flow to be computed was Meyer's, because velocity profiles from his calculation were readily available. For this flow, the Reynolds number based on $(r_o - r_i)$ is 400, the radius ratio is 5/6 ($\eta = r_i/r_o = \frac{5}{6}$), and the axial wavelength is 1.05 [$\lambda = 1.05(r_o - r_i)$]. The calculation was performed using 21 Fourier modes in the z direction and Chebychev polynomials through 21st order in the r direction (17 $\mathbf{u}^+$ and $\mathbf{u}^-$ functions). The nonlinear terms were computed on a 32×33 grid, thus eliminating aliasing. A disturbance to the laminar state was introduced and allowed to grow into steady-state Taylor vortices. In Fig. 2, the steady-state θ-velocity as a function of r is shown for the z location, where the normal velocity u_r is zero. Results of the present calculation and Meyer's 40×40 finite-difference calculations are shown; the agreement is very good. For the present calculation, the torque per unit length required to drive the inner cylinder (1.953×10^4) was within 0.6% of the value reported by Meyer (1.965×10^4).

Torque and stability calculations were performed for two geometries, a narrow gap where $\eta = 0.95$ and a wide gap where $\eta = 0.5$. These computations were done with nine Fourier modes and Chebychev polynomials through order 10, with nonlinear terms computed on a 16×17 grid. The disturbance wavelength in the z direction was assumed to be the wavelength corresponding to the minimum critical Reynolds number (2.009 and 1.988 for the narrow and wide gap, respectively [19]). The results of these calculations are summarized in Table I.

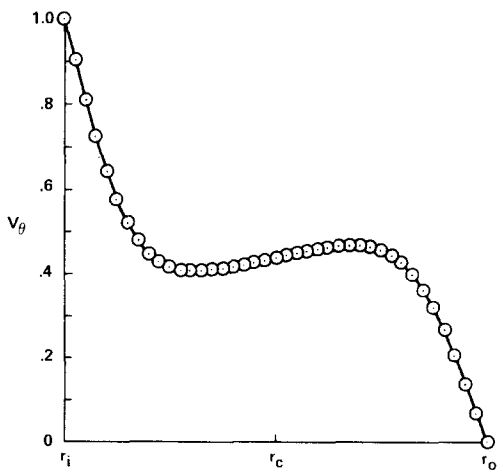

FIG. 2. Azimuthal velocity in Taylor–Couette flow (Re = 400, $\lambda = 1.05$, $\eta = 0.833$) as a function of r at the z location, at which radial velocity is zero. Shown are the present calculation (—) and the calculation of Meyer (O) [17]. r_i, r_c, r_o are inner cylinder, centerline and outer cylinder, respectively.

TABLE I

Results of Axisymmetric Calculations

	Critical Reynolds No.		Torque, G		
	Stability analysis [15]	Present calculation	Re	Experimental [19]	Present calculation
Narrow gap $\eta = 0.95$	184.99	185	195	5.26×10^5	5.42×10^5
Wide gap $\eta = 0.5$	68.19	68.2	78.8	1.479×10^3	1.487×10^3

The critical Reynolds number for transition to axisymmetric Taylor vortices was determined by searching for the Reynolds number at which a small disturbance neither decayed nor grew. A disturbance of the desired wavelength was added to the laminar solution, and the time evolution of the first Fourier coefficient was monitored. The disturbance would decay rapidly at first, until it consisted of only the least stable eigenmode; it would then either slowly grow or slowly decay, depending on whether the Reynolds number was above or below critical. Critical Reynolds numbers found in this way are presented in Table I; note that they are in excellent agreement with the analysis of DiPrima and Eagles [19] for both narrow-gap and wide-gap problems.

For the torque calculations, a disturbance to the laminar solution was allowed to grow to steady state. The nondimensional torque G (torque per unit length normalized by $\rho\nu^2$, where ν is the kinematic viscosity of the fluid) was computed from the formula

$$G = 2\pi r \,\mathrm{Re}\left(\frac{d}{dr}(r\bar{u}_\theta) - 2\bar{u}_\theta\right), \tag{42}$$

where the overbar denotes average over z. Comparison of these calculated torques in Table I with the data of Donnelly and Simon [18] should be made with some caution, for two reasons. First, the axial wavelength of the Taylor vortices in the experiment was not measured. The wavelength corresponding to minimum critical Reynolds number was used in the calculations as a good guess, because the Reynolds numbers are not far above the critical Reynolds numbers, and the experimental conditions were obtained by slowly increasing the speed of the inner cylinder from zero. Second, the experimental torque value in the subcritical regime are not in very good agreement with the torques predicted for laminar Taylor–Couette flow. This is especially true for the narrow-gap experiment, in which the experimental torque is consistently 3% below the theoretical value. For the wide-gap experiment, the data

are within 0.6% of the laminar torque for Reynolds numbers far below critical. In light of these considerations, the agreement of the present calculations with the experimental data of Donnelly and Simon is as good as can be expected (3% and 0.5% for narrow and wide gaps, respectively). In Fig. 3, contours of the secondary flow-stream function are plotted for the narrow-gap case, showing the familiar Taylor vortices.

The critical Reynolds number for the transition to nonaxisymmetric flow for the case $\lambda = 2.007$, $\eta = 0.877$, $m = 1$ (where the θ-wave length is $2\pi/m$), was determined as before by introducing a disturbance and allowing it to grow or decay. In this case, the base flow was Taylor vortices calulated with nine Fourier modes and Chebychev polynomials through tenth order. For the three-dimensional calculations, nine Fourier modes were used in the θ direction. The critical Reynolds number was found in this way to be 130, in good agreement with the value of 131 reported in [20]. The growth rate and fundamental frequency (precession speed), for an unstable nonaxisymmetric mode ($\mathrm{Re} = 177.6$, $\lambda = 2.007$, $\eta = 0.877$, $m = 6$) were found by allowing a small disturbance to develop until it consisted of only the unstable mode. Resulting values for growth rate (1.11×10^{-2}) and precession speed (2.54) are within 0.6% and 0.5%, respectively, of the values reported by Jones [20].

Fully developed wavy vortices ($\mathrm{Re} = 167$, $\lambda = 2.54$, $\eta = 0.877$, $m = 5$) were computed using nine Fourier modes in the θ and z directions and Chebychev polynomials through tenth order. Figure 4 shows contours of axial velocity at $r = 0.882 r_o$ (close to the inner cylinder), showing the wave in the θ direction. The calculated fundamental frequency of the flow was 2.16 ω_i, where ω_i is the inner-cylinder rotation frequency. This is in fair agreement with the value of 2.11 ω_i taken from Fig. 7 of [15].

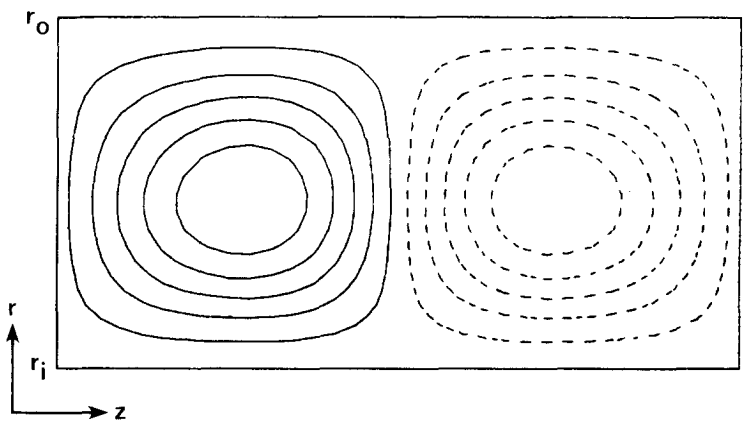

FIG. 3. Secondary flow stream-function contours for Taylor–Couette flow $\mathrm{Re} = 195$, $\lambda = 2.004$, $\eta = 0.95$). Solid lines are positive contours; dashed lines are negative contours.

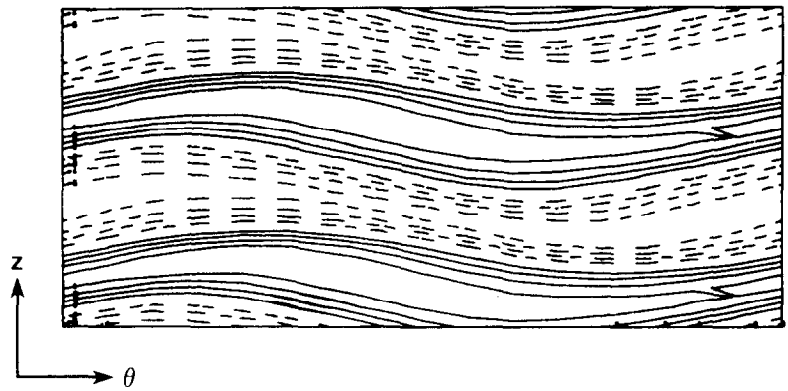

FIG. 4. Contours of axial velocity at $r = 0.822r_0$ for fully developed wavy vortices (Re = 167, $\lambda = 2.54$, $\eta = 0.877$, $m = 5$).

4.3 *Observations on Aliasing Errors*

Aliasing errors in the computation of the nonlinear terms are a potential problem in calculations with marginal resolution. In all of the calculations cited in Subsection 4.2, the nonlinear terms were computed using collocation grids large enough to eliminate aliasing by the $\frac{2}{3}$ rule. However, it is not clear what effect aliasing has, especially since the nonlinear terms are computed as $\mathbf{u} \times \boldsymbol{\omega}$, so in the absence of viscosity and time-differencing errors, kinetic energy is always conserved [21]. Several calculations were performed with and without aliasing, to determine what effects aliasing has in these problems.

The development of axisymmetric Taylor vortices (Re = 678.8, $\lambda = 2.35$, $\eta = 0.877$) from an initial disturbance has been computed in four ways: unaliased with 21×22 modes (Fourier modes $\times$ Chebychev modes); unaliased with 15×17 modes; unaliased with 9×11 modes; and aliased with 15×17 modes. Note that the 9×11 calculation was performed using a 16×17 collocation grid (as was the 15×17 aliased calculation), so that aliasing was removed by the $\frac{2}{3}$ rule. Plots of the time evolution of three of the Fourier–Chebychev coefficients are shown in Fig. 5. In Fig. 5a, note that the unaliased 15×17 and 21×22 calculations are in good agreement, indicating that they are approaching the exact solutions. The 9×11 unaliased calculation clearly has inadequate resolution, though it does exhibit some of the qualitative behavior of the more accurate solutions. The accuracy of the aliased calculation is poor; it exhibits qualitatively different behavior from that of the other cases. In Fig. 5b, the aliased calculation shows the correct qualitative behavior. Finally, in Fig. 5c, the aliased and 9×11 unaliased solutions are greatly different from each other and from the more accurate calculations. In Fig. 6, steady-state azimuthal velocity profiles at a particular z station are shown for the four calculations. Here the inadequacy of the 9×11 calculation is evident; however, the aliased solution is in fair agreement with the higher order calculations.

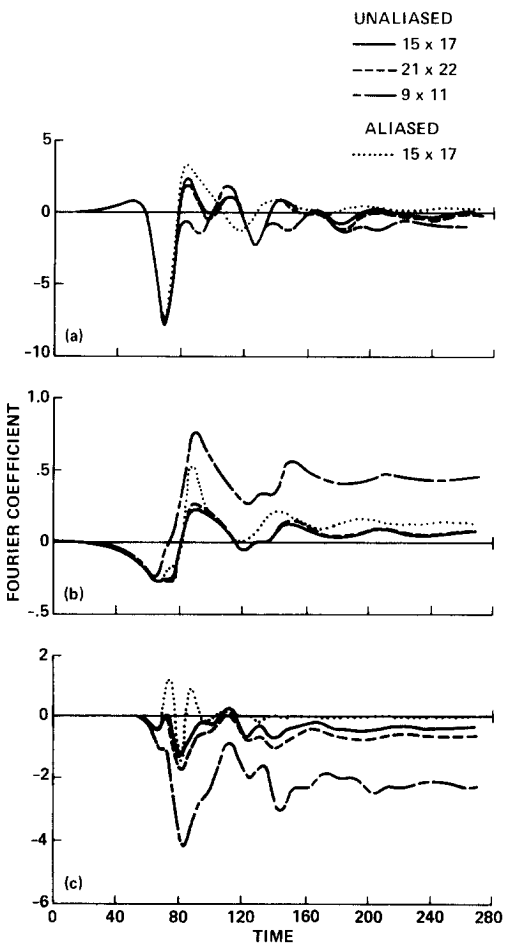

FIG. 5. History of Fourier coefficients after an initial disturbance to laminar Taylor–Couette flow (Re = 678.8, $\lambda = 2.35$, $\eta = 0.877$) for aliased and unaliased calculations. Coefficients are for (a) v_θ, T_1 term with $k_z = 2\pi/\lambda$, (b) v_z, T_7, $k_z = 2\pi/\lambda$, (c) v_z, T_1, $k_z = 8\pi/\lambda$.

From these observations, it appears that for the problem considered here, the effects of aliasing are more severe in transients than in steady state. In the steady state, the 15×17 aliased calculation is nearly as accurate as the 15×17 unaliased calculation. However, in the transient the 9×11 unaliased calculation and its 15×17 aliased counterpart are both unsatisfactory. This suggests that in time-dependent problems, aliasing errors could significantly degrade the accuracy of a calculation.

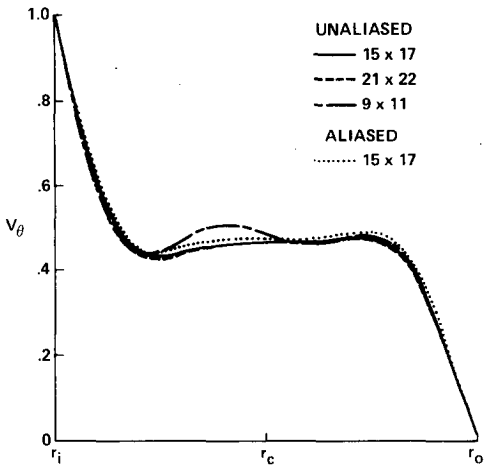

FIG. 6. Azimuthal velocity in Taylor–Couette flow ($\mathrm{Re} = 678.8$, $\lambda = 2.35$, and $\eta = 0.877$) as a function of r at the z location, at which the radial velocity is zero. Aliased and unaliased calculations are shown: r_i, r_c, and r_o are inner cylinder, center, and outer cylinder, respectively.

5. CONCLUSIONS

A spectral method for the solution of the Navier–Stokes equations for plane channel flow and flow between concentric cylinders has been presented. The method uses an expansion in vector functions which inherently satisfy the boundary conditions and the continuity equations. This has the advantage of treating the boundary and continuity constraints exactly and reducing the number of variables per spectral mode. Quasi-orthogonal functions have also been introduced that lead to banded matrices which are solved in $O(N)$ operations. These quasi-orthogonal functions have potential application in other problems.

The method has been used to compute the evolution of Tollmien–Schlichting waves in the channel and axisymmetric and three-dimensional Taylor vortices in Taylor–Couette flow. In all cases, agreement with available experimental and theoretical results has been very good.

REFERENCES

1. S. A. ORSZAG AND L. C. KELLS, *J. Fluid Mech.* **96** (1980), 159–205.
2. L. KLEISER AND U. SCHUMANN, *in* "Proceedings of the Third GAMM-Conference on Numerical Methods in Fluid Mechanics" (E. H. Hirschel, Ed.), pp. 165–173, Braunschweig, 1980.
3. A. T. PATERA AND S. A. ORSZAG, *J. Fluid. Mech.* **112** (1981), 467–474.
4. P. MARCUS, A. PATERA, AND S. A. ORSZAG, *in* "Proceedings of the Ninth International Conference on Numerical Methods in Fluid Mechanics," Aachen, 1982, to be published.
5. P. MOIN AND J. KIM, *J. Fluid Mech.* **118** (1982), 341–377.

6. P. MOIN AND J. KIM, *J. Comput. Phys.* **35** (1980), 381–392.
7. A. LEONARD, *Bull. Amer. Phys. Soc.* **26** (1981), 1247.
8. A. LEONARD AND A. WRAY, *in* "Proceedings of the Ninth International Conference on Numerical Methods in Fluid Mechanics," Aachen, 1982, to be published.
9. R. TEMAN, "Navier–Stokes Equations Theory and Numerical Analysis," North-Holland, Amsterdam/New York/Oxford, 1979.
10. A. T. PATERA AND S. A. ORSZAG, *in* "Proceedings of the Seventh International Conference on Numerical Methods in Fluid Mechanics" (W. C. Reynolds and R. W. MacCormack, Eds.), Springer-Verlag, Berlin/Heidelberg/New York, 1980.
11. J. T. STUART, Hydrodynamic Stability, *in* "Laminar Boundary Layers" (L. Rosenhead, Ed.), Chap. 9, Oxford Univ. Press, London/New York, 1963.
12. D. GOTTLIEB AND S. A. ORSZAG, "Numerical Analysis of Spectral Methods," NSF-CBMS Monograph, No. 26, Society of Industrial Applied Mathematics, Philadelphia, 1977.
13. L. FOX AND I. B. PARKER, "Chebychev Polynomials in Numerical Analysis," Oxford Univ. Press, London/New York, 1968.
14. L. H. LEE AND W. C. REYNOLDS, *Quart. J. Mech. Appl. Math.* **20** (1967), 1.
15. D. COLES, *J. Fluid. Mech.* **21** (1965), 385–425.
16. P. R. FENSTERMACHER, H. L. SWINNEY, AND J. P. GOLLUB, *J. Fluid Mech.* **94** (1979), 103–128.
17. K. A. MEYER, "A Two-Dimensional, Time-Dependent Numerical Study of Rotational Couette Flow," Dissertation, Stanford Univ., Stanford, Calif., 1966.
18. R. J. DONNELLY AND N. J. SIMON, *J. Fluid. Mech.* **7** (1960), 401–418.
19. R. C. DIPRIMA AND P. M. EAGLES, *Phys. Fluids* **20** (1977), 171–175.
20. C. A. JONES, *J. Fluid Mech.* **102** (1981), 249–261.
21. N. N. MANSOUR, P. MOIN, W. C. REYNOLDS, AND J. H. FERZIGER, *in* "Turbulent Shear Flows I" (F. Durst, B. E. Launder, and F. W. Schmidt, Eds.), pp. 379–385, Springer, New York, 1979.